Thermogravimetric characterisation and kinetic analysis of Nannochloropsis sp. and Tetraselmis sp. microalgae for pyrolysis, combustion and oxy-combustion

Thermogravimetric characterisation and kinetic analysis of Nannochloropsis sp. and Tetraselmis sp. microalgae for pyrolysis, combustion and oxy-combustion

Federica Dessì[1,*], Mauro Mureddu[1], Francesca Ferrara[1], Javier Fermoso[2,3], Alessandro Orsini[1], Aimaro Sanna[2], Alberto Pettinau[1]

[1] Sotacarbo S.p.A., Grande Miniera di Serbariu, 09013 Carbonia, ITALY

[2] Advanced Biofuels Lab, Institute of Mechanical, Process and Energy Engineering, Heriot-Watt University, EH14 4AS, Edinburgh, UNITED KINGDOM

[3] Thermochemical Processes Unit, IMDEA Energy, Avda. Ramón de la Sagra 3, 28935, Móstoles, Madrid, SPAIN

[*] Corresponding authors: federica.dessi@sotacarbo.it;

Abstract

This paper reports the results of a complete kinetic study, based on thermogravimetric characterisation, to compare the performance of *Nannochloropsis* sp. and *Tetraselmis* sp. microalgae during pyrolysis and combustion with air, enriched air and oxygen. The analysis has been carried out including both the single- and multi-step approach studying the effect of different model-free methods and heating rates. In addition, the study brings together the pseudo-components (obtained by peaks deconvolution) model

and master plot methodology to discriminate the kinetic model followed by the different processes with the aim to determine the kinetic triplet (activation energy, reaction order and pre-exponential factor). It results that the thermal decomposition of the microalgae cannot be represented by a single reaction mechanism for the whole conversion range, but several parallel decomposition reactions have been taken into account, and the kinetics have been assessed from each decomposition kinetic of the pseudo-components. The kinetic profiles can be interpreted as the combined effects of reaction-order (*F*), nucleation (*A*), exponential nucleation (*P*) and geometrical contraction (*R*) mechanisms.

Keywords: Nannochloropsis; Tetraselmis; Microalgae; Thermogravimetric analysis; Kinetic analysis.

1. Introduction

Cutting anthropogenic carbon dioxide (and other greenhouse gases) emissions to zero in just few decades is universally recognized as the only way to contain the alteration of Earth's climate. To achieve this objective without compromising the current standards of living, it is essential to address the problem on several fronts: a significant reduction of energy waste, with a gradual but quick revision of energy management concept in civil, industrial, transport and power generation sectors; the development of low carbon energy technologies, such as carbon dioxide capture, utilization and storage (CCUS); and a wide exploitation of renewable energy sources [1]. But the diffusion of intermittent renewable sources (mainly wind and solar) makes grid regulation increasingly

challenging because utilities must balance ever changing electrical loads with ever changing, non-programmable generation [2].

In this respect, biomass can play a very important role, since its supply and use are basically free from the problem of intermittency [3]. It can be directly used as a fuel for heat and power generation – possibly in combination with CO_2 capture and storage technology (the so-called bio-energy carbon capture and storage, BECCS) for a negative carbon balance [4] – or as a feedstock for the production of biofuels or other products [5,6].

Microalgae are particularly interesting biomasses due to some key aspects such as abundant distribution, fast growth, high production rate, and high photosynthetic or carbon fixing efficiency [7]. Moreover, differently from other biomass, microalgae are cultivated in water – including wastewater as nutrient sources, avoiding the use of arable land [8]. Nowadays, microalgae are generally marketed as nutritional supplements but they are also promising for power generation and biofuels [9] and biopolyols production, due to the high lipids (especially triglycerides) content and yield [10].

Among microalgae, *Nannochloropsis* sp. and *Tetraselmis* sp. are widely studied in the scientific literature. Alimentary utilisation aside, biodiesel production is definitely the most common subject of these studies, with a wide number of researches focused on different extraction methods [11], in particular for *Nannochloropsis* sp. [12]. Several studies are also available on pyrolysis and co-pyrolysis of microalgae [13,14,15], as well as on hydrothermal liquefaction [16,17]. Pyrolysis kinetic of both the above-mentioned microalgae is assessed by Ceylan and Kazan [18] and particular attention is also paid

on catalytic pyrolysis, with few interesting experimental studies [19]. Catalytic pyrolysis is also considered as an option for bio-oil production [20]. And a wide interest is paid on co-pyrolysis of microalgae with coal [21,22], other biomasses [23], and plastics [24], with particular reference to the synergistic effects of the fuels. Several studies are also focused on microalgae as a direct combustion fuel [25,26], and just few studies consider oxy-combustion as a possible option for power generation from microalgae – especially *Chlorella* sp. – and their blends with other fuels [27]. One of the key issues in utilising biomass feedstocks (both lignocellulosic and micro- or macro-algal) as a solid fuel for energy generation is the occurrence of ash-related problems in boilers [28,29]. Biomass materials, especially agricultural residues, are known to be rich in alkali metals such as Na and K and these alkali metals can cause undesirable slagging and fouling in the high temperature furnaces and boilers due to the formation of low melting- or softening-point alkali silicates [30,31]. Moreover, the ash content and its chemical composition have an influence on the application of combustion technology. The ash-related issues are taking on during the modelling and designing of the reactor. Therefore, to make biomass thermal conversion processes effective, shapes, sizes, and compositions, as well as the characteristics of the parent material, must be clearly studied. To the best of the authors' knowledge, no works dealing with a comparison between microalgae pyrolysis, gasification and combustion performance have been published so far. Besides, pyrolytic and combustion kinetic behaviour of microalgae has been widely studied by using global and semi-global kinetic mechanism. The single-step mechanism is by far the most employed global kinetic model [32,33]; here, the biomass is considered to be composed of a single pseudo-component. On the other hand, this

mechanism is very simple, and it lacks its application in describing various steps of decomposition during pyrolysis or combustion process due to the compositional variability and complex nature of the biomass [34]. Among the kinetic fitting models, multiple parallel reaction models can be used to describe microalgae decomposition. These models were originally developed to characterise the pyrolysis of the three main components of lignocellulosic biomass, *i.e.*, hemicellulose, cellulose and lignin [35]. In the independent parallel reaction kinetic model, every pseudo-component degrades independently and the overall biomass pyrolysis or combustion can be obtained by superimposing decomposition of all pseudo-components [36]. Because microalgae contain lignocellulosic components in their cell wall structure in addition to carbohydrates, proteins and lipids, the decomposition behaviour of this complex material cannot be closely described using simple models [37]. Furthermore, most of the studies on the pyrolysis kinetics of microalgae available in the literature are based on a reduced number of thermogravimetric curves and, due to the limited number of investigation points on which they are based, these kinetic models cannot provide information about the fit quality of the models [38]. To the authors' knowledge, very few papers deal with considering the pseudo-components model have been published so far. There is an interesting study carried out by Ali and Bahadar [39], where the thermogravimetric pyrolysis behaviour of *Sargassum* sp. macroalga was evaluated using the pseudo-components model; however, an in-depth study on the determination of the kinetic triplets (activation energy, E_a, reaction order, n, and pre-exponential factor, A) was not taken into account.

With the aim to cover this gap, this paper compares, from the kinetic point of view, the performance of *Nannochloropsis* sp. and *Tetraselmis* sp. microalgae during pyrolysis (considered as a benchmark) and combustion with air, enriched air and oxygen in view of a possible BECCS application. In particular, in addition to air-blown combustion coupled with post-combustion CO_2 capture and oxy-fuel combustion, the so-called "partial oxy-combustion" (with air enriched in oxygen) has been considered: this is a hybrid approach that could allow to reduce the size and enhance the performance of post-combustion CO_2 capture – with lower energy penalties – by reducing flue gas dilution [40,41].

For the first time, this work carries out a complete kinetic study, brings together the pseudo-components model and master plot methodology – applied to each of the pseudo-components – to discriminate the kinetic model followed by the different processes with the aim to determine the kinetic triplet: the activation energy, the pre-exponential factor and the reaction model. Meanwhile, the effect of different model-free methods and heating rate on the accuracy of the master plot method has been discussed.

2. Materials and methods

2.1. Microalgae

The analysis here reported is focused on two different microalgae, *i.e. Nannochloropsis sp.* (*Na*) and *Tetraselmis sp.* (*Te*). In particular, *Na* is a microalga characterised by a high level of polyunsaturated fatty acids that makes it an excellent food additive to human nutrition and a feedstock for bio-fuels production. On the other hand, *Te* is an

alga within the order *Chlorodendrales* and is one of the key components of phytoplankton.

Microalgae *Na* (Nanno 3600) and *Te* (Tetra 3600) have been provided by Varicon Aqua Solutions (Worcester, UK) in liquid form (18.4% dry weight). The algae that were produced by Reed Mariculture Inc (USA) as standard shellfish food, were dried in oven at 50 °C for 72 h, pulverized using a pestle and mortar to <500 μm and stored in a desiccator for further use.

2.2. Sample preparation and preliminary analyses

Both *Na* and *Te* samples have been initially dried in an oven with a constant temperature of 107 ± 2 °C for 24 h. They resulted in a greenish/yellowish powder that has been repeatedly grinded with pestle to disaggregate the small agglomerates and sieved with a 250 μm mesh, in order to obtain representative samples, stored in desiccators to prevent moisture absorption from the atmosphere. Each sample is preliminarily characterised by proximate, ultimate and calorimetric analyses (Table 1). The analyses are carried out in the Sotacarbo laboratories according to the international standards. In particular, proximate analysis is performed by a LECO TGA-701 thermogravimetric analyser; ultimate analysis is carried out on a LECO Truspec CHN/S analyser; finally, the energy content of the sample is measured using an adiabatic oxygen bomb calorimeter by a LECO AC-500 calorimeter. All the measurements have been replicated three times to decrease the error of the experimental results and to determine their reproducibility.

Table 1. Proximate, ultimate and calorimetric analyses of microalgae.

	Nannochloropsis	*Tetraselmis*	*Relative standard deviation*	*Standard*
Proximate analysis (% by weight, dry basis)				
Fixed carbon	4.44	7.94	0.02%	By difference
Moisture	0.20	0.27	0.02%	ASTM D 5142-04
Volatiles	81.00	70.51	0.02%	ASTM D 5142-04
Ash	14.36	21.28	0.02%	ASTM D 5142-04
Ultimate analysis (% by weight, dry basis)				
Total carbon	45.40	38.70	0.5%	ASTM D 5373-02
Hydrogen	5.19	4.30	1.0%	ASTM D 5373-02
Nitrogen	8.60	6.63	0.5%	ASTM D 5373-02
Sulphur	0.21	0.26	1.0%	ASTM D 4239-05
Oxygen[(1)]	26.24	28.83	-	By difference
Ash	14.36	21.28	0.02%	ASTM D 5142-04
Higher heating value (MJ/kg)				
Higher heating value	16.31	12.61	0.05%	ISO 1928:1995

[(1)] By difference

Both species show some difference in primary fuel characterisation. It is worth nothing the high volatiles content in both the microalgae (approximately 70-80% by weight). The ash content of both the microalgae is very high (14.4 and 21.3% by weight for *Na* and *Te*, respectively). Generally, the ash content of microalgae is higher than that of lignocellulosic biomass due to the facts that microalgae species are constantly exposed to minerals during the cultivation process, *i.e.* submerged in water containing a considerable amount of mineral matter, which diffuse into the algae cells [42]. Higher ash content would affect the designing and operation process causing slagging, fouling and other ash-related problems during conversion process but can be used as a catalyst material for biochar formation [43]. In terms of elemental composition, the carbon (45–39 wt.% for *Na* and *Te*, respectively) and hydrogen (5–4 wt.%) contents are similar to those of lignocellulose. On the other hand, oxygen (26–28 wt.%) and nitrogen (8–7 wt.%) contents are lower and much higher, respectively, compared to lignocellulosic biomass [44]. Wang and Brown [45] stated that the nitrogen constituents of microalgae may include chlorophyll, nucleic acids, and glucosamides along with cell

wall materials. Due to thermal decomposition of nitrogen-containing compounds, such as proteins, formation of pyrolysis products with nitrogen contents could be expected [46]. Moreover, ultimate analysis shows a lower carbon content – especially for *Te* – than that of lignocellulosic biomass; this results in a reduction of the calorific value from 16.3 MJ/kg to 12.6 MJ/kg for *Na* and *Te*, respectively. Based on the nitrogen content, the proteins amount (53.75 and 41.44% by weight for *Na* and *Te*, respectively) has been estimated using a nitrogen factor (NF) of 6.25 from the following equation [47]:

$$\text{Proteins (wt.\%)} = \text{Nitrogen (wt.\%)} * NF \quad (1)$$

2.3. Experimental procedures

Biomass characterisation by thermogravimetric analysis (TGA) has been carried out by using the Mettler Toledo TG/DSC3+. Each fuel sample (about 8 mg, loaded into a 70 µl alumina crucible) is heated up from ambient temperature to 1100 °C at different heating rates, *i.e.* 5, 10, 15, 20 and 40 °C/min (according to the International Confederation for Thermal Analysis and Calorimetry “ICTAC” for a reliable determination of the Arrhenius parameters [48]). Blank experiments are carried out to obtain the baselines, used to subtract the buoyancy effect, calibrating the experiments with samples. All the samples are analysed under exactly the same conditions and each experiment is replicated three times to decrease the error of the experimental results and to determine their reproducibility. The pyrolysis process is assessed in an inert atmosphere, fluxing samples with 50 ml/min of pure nitrogen (99.999 vol.%) provided in pressurized cylinders. Combustion tests are carried out in an oxidizing environment, with 100 ml/min of a mixture of oxygen and nitrogen characterised by an oxygen concentration of 21, 58 and 95 vol.% to simulate air, enriched air (partial oxy-combustion) and oxy-combustion,

respectively, the latter being the typical oxygen purity downwards of a conventional air separation unit (ASU) [41]. For the sake of simplicity, these regimes are indicated as PYR (pyrolysis, 99.999 vol.% of N_2), ABC (air-blown combustion, 21 vol.% of O_2), POX (partial oxy-combustion, 58 vol.% of O_2), FOX (full oxy-combustion, 95 vol.% of O_2).

The raw experimental results are expressed in terms of thermogravimetric (TG) and differential thermogravimetric (DTG) profiles.

2.4. Kinetic models

According to a previous study by the authors [49], the activation energy has been calculated as a function of the instantaneous conversion and/or temperature, on the basis of the classical integral methods [50], *i.e.* the so-called Flynn-Wall-Ozawa (FWO) [51,52], Kissinger-Akahira-Sunose (KAS) [53,54], Starink [55] and Kissinger methods [56] (Table 2). In addition, the master plot method has been used to identify the mechanism of solid-state reaction and to determine, from the knowledge of the most probable reaction mechanism $f(\alpha)$ (Table 2), the values of the reaction order n and the pre-exponential factor A. The master plot has been built up by comparing experimental and theoretical master plots, according to the method proposed by [57].

Table 2. Most common kinetic models of solid-state processes [58].

Model-free method	*Slope-Intercept form: y=mx+q*
Flynn-Wall-Ozawa (FWO)	$ln\beta_i = ln\left(\frac{A\,E_{a,\alpha}}{R\,g(\alpha)}\right) - 5.331 - 1.052\,\frac{E_{a,\alpha}}{R\,T_{\alpha,i}}$
Kissinger–Akahira–Sunose (KAS)	$ln\left(\frac{\beta_i}{T_{\alpha,i}^2}\right) = ln\left(\frac{A\,R}{E_{a,\alpha}\,g(\alpha)}\right) - \frac{E_{a,\alpha}}{R\,T_{\alpha,i}}$
Starink	$ln\left(\frac{\beta_i}{T_{\alpha,i}^{1.92}}\right) = Const - 1.0008\frac{E_\alpha}{R\,T_{\alpha,i}}$
Kissinger	$ln\left(\frac{\beta_i}{T_m^2}\right) = ln\left(\frac{A\,R}{E_a}\right) - \frac{E_a}{R\,T_m}$

Master Plot method		
Integral form	$\frac{g(\alpha)}{g(0.5)} = \frac{P(u)}{P(u_{0.5})}$	$g(\alpha) = \frac{A\,E}{\beta\,R}P(u)$
Doyle's approximation	$P(u) = 0.00484\exp(-1.0516\,u)$	$u = \frac{E_a}{R\,T}$

Reaction mechanism	*Symbol*	*Differential form, f(α)*	*Integral form, g(α)*
Reaction-order			
First order	F1	$(1-\alpha)$	$-ln(1-\alpha)$
Second order	F2	$(1-\alpha)^2$	$(1-\alpha)^{-1} - 1$
Third order	F3	$(1-\alpha)^3$	$\frac{1}{2}[(1-\alpha)^{-2} - 1]$
n-th order	Fn	$(1-\alpha)^n$	$\frac{1}{(n-1)}[(1-\alpha)^{-(n-1)} - 1]$
Diffusion			
One-way transport	D1	$\frac{1}{2}\alpha$	α^2
Two-way transport (Valensi)	D2	$[-ln(1-\alpha)]^{-1}$	$\alpha + (1-\alpha)\,ln(1-\alpha)$
Three-way transport (Jander)	D3	$\frac{3}{2}\left(1-\alpha\right)^{\frac{-2}{3}}\left[1-(1-\alpha)^{\frac{1}{3}}\right]^{-1}$	$\left[1-(1-\alpha)^{\frac{1}{3}}\right]^2$
Three-way transport (Ginstling-Brounshtein)	D4	$\frac{3}{2}\left(1-\alpha\right)^{\frac{-1}{3}} - 1\Big)^{-1}$	$\left(1-\frac{2\alpha}{3}\right) - (1-\alpha)^{\frac{2}{3}}$
Geometrical contraction			
One dimension	R1	1	α
Two dimensions (contracting cylinder)	R2	$2(1-\alpha)^{\frac{1}{2}}$	$1 - (1-\alpha)^{\frac{1}{2}}$
Three dimensions (contracting sphere)	R3	$3(1-\alpha)^{\frac{2}{3}}$	$1 - (1-\alpha)^{\frac{1}{3}}$
Nucleation			
Two dimensional (Avrami-Erofeev)	A2	$2(1-\alpha)[-ln(1-\alpha)]^{\frac{1}{2}}$	$[-ln(1-\alpha)]^{\frac{1}{2}}$
Three dimensional (Avrami-Erofeev)	A3	$3(1-\alpha)[-ln(1-\alpha)]^{\frac{2}{3}}$	$[-ln(1-\alpha)]^{\frac{1}{3}}$
Exponential nucleation			
Power law, n=1/2	P2	$2\alpha^{\frac{1}{2}}$	$\alpha^{\frac{1}{2}}$
Power law, n=1/3	P3	$3\alpha^{\frac{2}{3}}$	$\alpha^{\frac{1}{3}}$
Power law, n=1/4	P4	$4\alpha^{\frac{3}{4}}$	$\alpha^{\frac{1}{4}}$

For the single-step reaction mechanism approach, first, the conversion has been calculated from the weight of the sample, considering $\alpha=0$ and $\alpha=1$ in correspondence of initial and final temperature of the process (ambient temperature and 1100 °C), respectively. Subsequently, the values of E_a are calculated using the model-free methods (FWO, KAS and Starink), while the values of $f(\alpha)$ and A have been obtained using the integral master plot method. As reported by Vyazovkin [59], the application of the master plot is contingent on E_a invariable with respect to conversion degree. Therefore, to calculate the experimental master plot, the average value of activation energy obtained with model-free methods has been used. All methods have been implemented using Microsoft Excel® software. The kinetic results described below indicate that the use of a single-step mechanism reaction often does not allow to characterise the microalgae decomposition process in the whole conversion range.

Consequently, several parallel decomposition reactions have been be taken into account, and the kinetic has been assessed from each decomposition kinetics of the pseudo-components, according to [34], with so-called multi-step reaction mechanism approach. In this procedure, each estimated curve is related to a possible component of the microalgae decomposition in pseudo-component. The pseudo-components decomposition curves have been obtained by using the Multiple Peak Fit tool of Origin Pro® software through the non-linear peak fitting using the iteration algorithm of Levenberg-Marquardt and the Gauss function equation. The kinetic parameters are obtained separately for each deconvoluted profile by Kissinger and master plot methods and, consequently, by calculating a value of E_a and A and $f(\alpha)$ at the maximum value of the reaction, using Microsoft Excel® software. The conversion for pseudo-components

has been calculated considering α=0 and α=1 in correspondence of the initial and final temperature of each DTG deconvolution profile.

3. Results and discussion

The results of the study on *Na* and *Te* are here reported in terms of thermogravimetric behaviour, kinetic analysis (determined by both single and multiple step mechanisms) and the evaluation of the reaction mechanism.

3.1 Thermogravimetric behaviour of pyrolysis, combustion, partial and full oxy-combustion

Pyrolysis, combustion, partial oxy-combustion and full oxy-combustion profiles for the *Na* and *Te* microalgae are shown in Figure 1, which illustrates the weight loss curve (TG) and the derivative thermogravimetric (DTG) evolution profiles obtained at a heating rate of 20 °C/min (chosen as reference rate for this study).

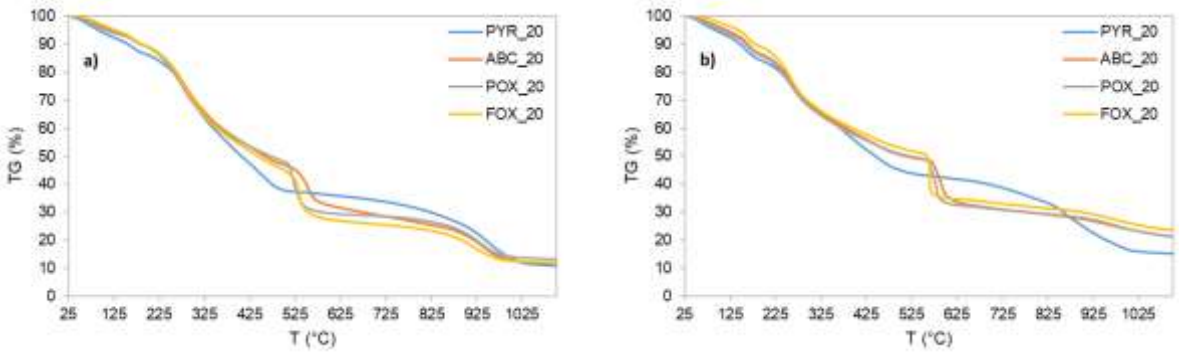

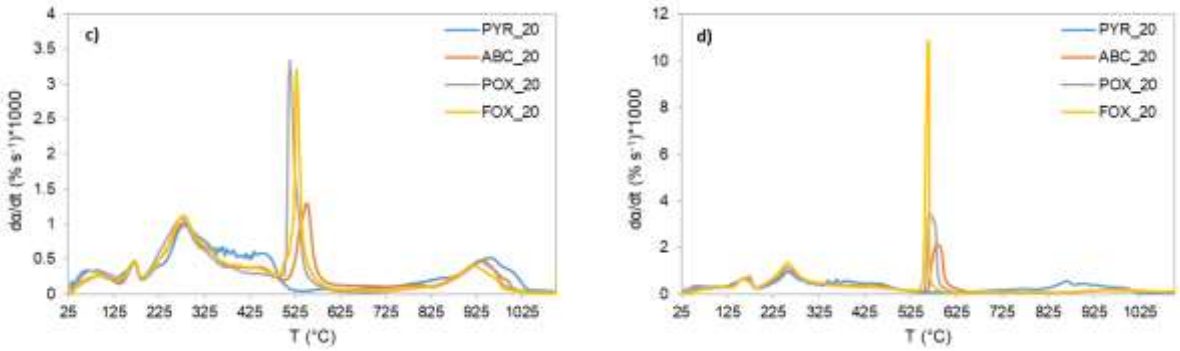

Figure 1. TG (a and b) and DTG curves (c and d) of Na (left side) and Te (right side), at 20 °C/min.

Regardless the kind of process (*i.e.* pyrolysis, combustion, partial oxy-combustion and full oxy-combustion), the average remaining mass for *Na* at 1100 °C is estimated to be 12 wt.%, which is slightly lower than that of *Te* in pyrolysis regime (15 wt.%) and considerably lower than that of *Te* in partial and full oxy-combustion processes (approximately 22 wt.%). The whole of the above TG results indicates that the overall weight loss is significantly higher for *Na* with respect to *Te*. TG and DTG profiles show that the first decomposition step is not influenced by the oxygen concentration as the curves almost overlap. This phenomenon is attributed to the thermal decomposition of the sample that occurs in the kinetic control zone, being mainly affected by the temperature, and the effect of oxygen concentration is almost negligible [60]. Nevertheless, it has not been observed any significant overall mass loss of Na and Te as a function of oxygen concentration. It is worth noting that the higher oxygen concentration (95 vol.%) slightly shifts TG and DTG curves to the low temperature area (Figure 1) for both the microalgae samples, indicating the advance in combustion and complete combustion at lower temperatures and effectively enhancing the reaction rate

during the heating process. According to different studies [61,62], these results can be attributed to the diffusion control zone during the combustion reaction where oxygen concentration becomes the major influencing factor. The dissimilar shape of the TG and DTG curves of both the microalgae suggests a remarkable difference between the pyrolysis and combustion (including partial and full oxy-combustion) processes. On the whole, three main degradation steps common to all the operative conditions can be observed. The first stage (up to 180 °C) associated with a small weight loss due to dehydration phase (cellular water, external physisorbed water and light hydrocarbons) is observed for the two samples at every operative condition. The second stage represents the main devolatilization reactions, where most of the sample weight is lost as volatile matter (180-500 °C). Different shoulders can be distinguished in this stage, being the low-temperature peak (*ca*. 180-320 °C) mainly associated to the degradation of carbohydrates and soluble polysaccharide, whereas the higher temperature peaks (*ca*. 320-500 °C) would correspond to the degradation of proteins and lipids, other insoluble polysaccharides and crude lipids [21]. Finally, the last stage takes place at temperatures above 500 °C for all the combustion regimes (21, 58 and 95 vol.% of oxygen), and above 700 °C for the pyrolysis process leading to char formation and solid residue decomposition [63]. Moreover, from the DTG point of view (Figure 1c and 1d), the differences between pyrolysis and all the combustion regimes are clear. In particular, it is possible to observe the lack of the narrow and high intensity peak centred at *ca.* 520 °C for the pyrolysis of both *Na* and *Te* microalgae, found for all the combustion regimes, associated with the oxidation of char; a similar trend has been reported by several authors [64], which focus on the evolved gases from the

thermochemical conversion of *Nannochloropsis gaditana* microalga. Furthermore, during combustion of Te in the temperature region of 820-1100 °C, the oxidation of inorganic compounds does not seem taking place.

Thanks to the thermogravimetric analysis extended up to 1100 °C – never reported in this kind of works – the presence of a significant and non-negligible peak at high temperature (from 800 to 1000 °C) has been detected, ascribed to char formation and decomposition of inorganic material [65,66]. From proximate analysis (Table 1) is it possible to observe the high ash content for both the samples, mainly due to the high alkali metal content in the feedstock [66]. Previous studies [67,68] indicate that the presence of sodium, potassium, magnesium and silicate in ash significantly affects pyrolysis degradation of biomass material, while potassium, sodium, calcium and magnesium are the main components influencing the combustion process. According to the findings of Figure 1c and 1d, decomposition of inorganic compounds (metal carbonates and sulfates) can be linked to the peak at *ca.* 900 °C for both the microalgae. On the contrary, a different behaviour can be noticed for *Te* sample, in which only the pyrolysis process influences the decomposition of inorganic compounds as evidenced by the peak located at 900 °C, which is instead absent for the partial- and full oxy-combustion.

Figures S1, S2, S3 and S4 (Supplementary material) show TG and DTG curves obtained at different heating rates (β = 5, 10, 15 and 40 °C/min) in both pyrolysis, combustion, partial and full oxy-combustion modes for the two microalgae. For both the samples, independently from the operative conditions, the main peak shifts slightly towards a higher temperature with the increase of β due to heat transfer limitation,

showing that an increase of heating rate tends to postpone the thermal decomposition process. This can be reasonably attributed to the fact that the heating of solid particles occurs more gradually at lower heating rates, thus leading to an improved and more effective heat transfer to the inner portions and among the particles.

According to the literature, the above results allow to observe that the main decomposition step is actually a very complex process, involving at least three or more overlapped steps, such as the shoulders and the overlapped peaks revealed in the DTG profiles.

3.2 Kinetic analysis and results

3.2.1 Kinetic parameters determined for the single-step mechanism

The activation energy for the conversion range 0.05-0.95, by FWO, KAS and Starink methods in pyrolysis, combustion, partial and full oxy-combustion, has been calculated for both the microalgae. From the linearization of the plots at different heating rates, the E_a values and the corresponding correlation coefficients (R^2) have been obtained at various conversion degrees, and reported in Tables S1, S2, S3, S4, S5, S6, S7 and S8. The values of R^2 indicate a good reliability of the results in the entire conversion range. The variation trend of activation energies with proceeding conversion are similar for FWO, KAS and Starink methods. Nevertheless, for each kinetic regime, the E_a values show a great dispersion without a precise trend. This behaviour is related to simultaneous decomposition of proteins, carbohydrates and lipids. As mentioned in the previous section, the thermal reactivity of proteins and carbohydrates is greater than lipids, so the decomposition occurs at lower temperatures. Lipids degradation needs

more energy and higher temperatures. In line with these assumptions, an increase in activation energy with progressing of conversion has been observed during the analysis (Figure 2). The last stage, which leads to char formation and solid residue decomposition, involves an increase in activation energy [69]. Figure 2 shows the comparison between conversion rate *(dα/dt)* of each microalga, at 20 °C/min, and the activation energy (determined with FWO, KAS and Starink methods) at various conversion degrees and different regimes. It can be observed that the activation energy tends to vary in correspondence with the peaks of the pseudo-components. The behaviour proves that there is more than one single reaction mechanism [70] in both microalgae.

As shown in Table 3, the average values of activation energy solved by model-free methods are very close to each other. Therefore, the average values of three methods have been expressed as activation energy of *Na* and *Te*: 163.2 and 124.0 kJ/mol for pyrolysis, 104.54 and 132.12 kJ/mol for combustion, 130.87 and 207.66 kJ/mol for partial oxy-combustion, 113.14 and 256.38 kJ/mol for full oxy-combustion. These results indicate that the activation energy of *Te* increases with increased oxygen concentration [60]. Fang et al. [71] suggested that the activation energy is affected by the decrease of activated molecule concentration, diffusion limitation and organic impurities during the pyrolysis and combustion processes. Indeed, as oxygen concentration increases, heat released from semi-coke oxidization increases and thus increases surface temperature of semi-coke. The semi-coke structure expands the size of grain and increases ash content [60]. Consequently, the activation energy increases. Unlike of the *Te*, the activation energy of *Na* changed remarkably from pyrolysis to combustion and from

partial to full oxy-combustion processes. Munir et al. [72] suggest that this is due to higher char combustion rate, which might relate to heterogeneous structure and mutual interaction of the individual components, less char conversion time and higher reactivity in presence of external oxygen.

Table 3. Average values of activation energy of Na and Te in pyrolysis, combustion, partial and full oxy-combustion processes calculated by different model-free methods.

Process	*Sample*	*FWO method*		*KAS method*		*Starink method*	
		E_a *(kJ/mol)*	R^2	E_a *(kJ/mol)*	R^2	E_a *(kJ/mol)*	R^2
PYR	Na	165.33	0.848	159.92	0.813	164.33	0.822
	Te	127.40	0.833	120.54	0.801	124.07	0.804
ABC	Na	108.38	0.921	101.56	0.894	103.70	0.897
	Te	138.21	0.857	127.24	0.810	131.11	0.811
POX	Na	130.32	0.899	130.71	0.867	131.59	0.878
	Te	201.22	0.723	210.55	0.733	211.22	0.740
FOX	Na	116.50	0.836	110.45	0.809	112.48	0.813
	Te	249.55	0.849	258.00	0.852	261.61	0.855

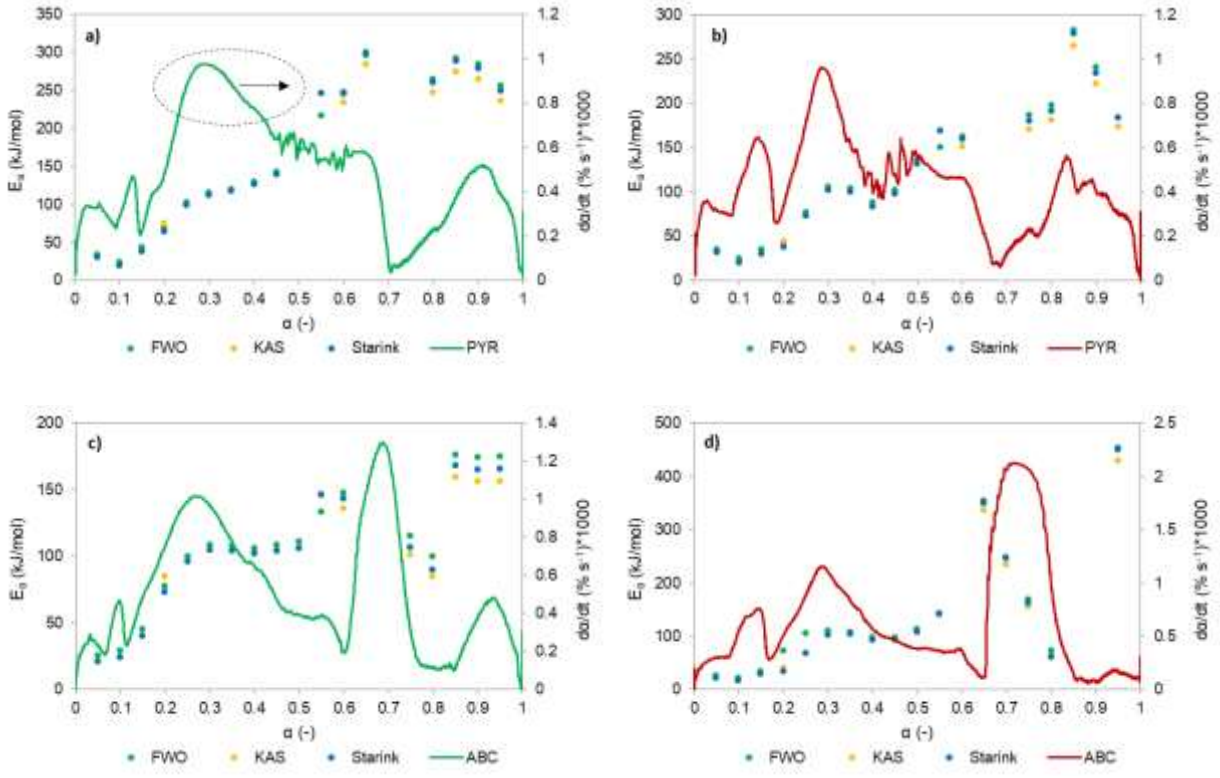

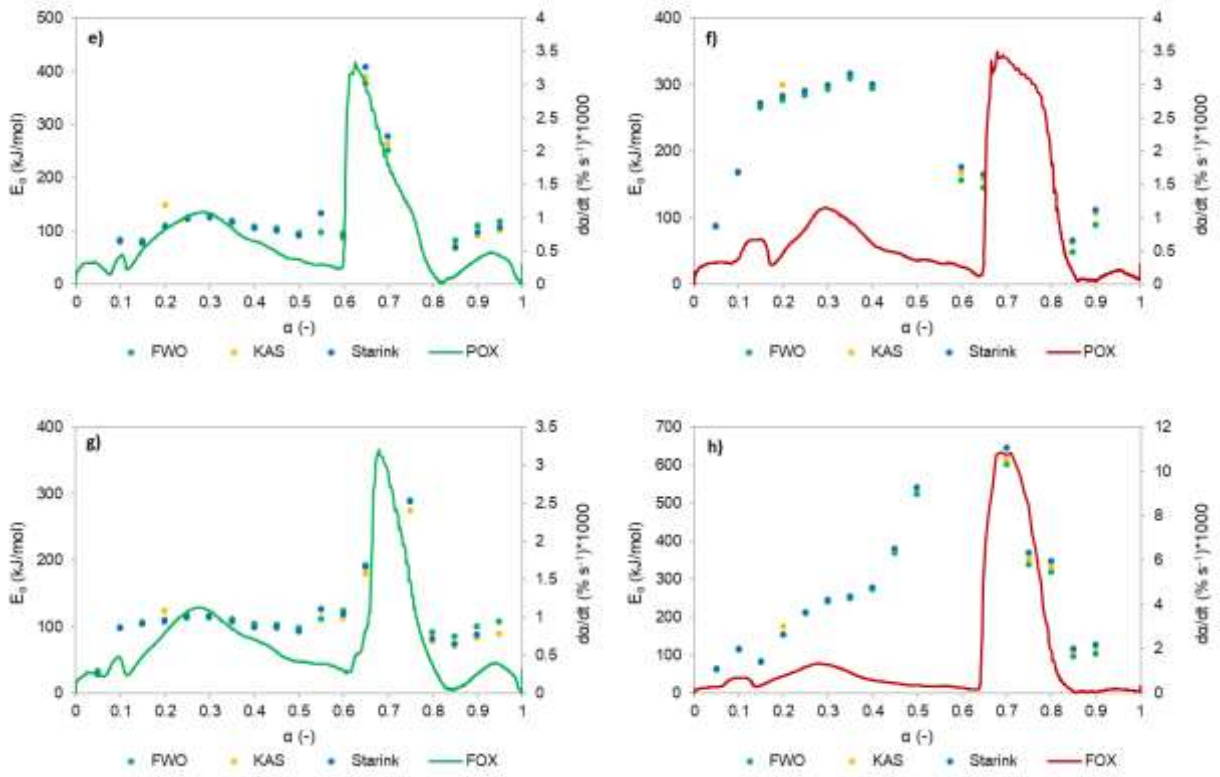

Figure 2. Comparison between activation energy, calculated by FWO, KAS and Starink method, and conversion rate of Na (left side) and Te (right side) in pyrolysis (a and b), combustion (c and d), partial oxy-combustion (e and f) and full oxy-combustion (g and h) processes, at 20 °C/min.

Figure 3 shows the theoretical and experimental master plots of *Na* and *Te* samples under pyrolysis conditions during the conversion change. The curves are represented by theoretical integral master plot $g(\alpha)/g(\alpha)_{0.5}$ (reaction order “F”, nucleation “A”, exponential nucleation “P”, geometrical contraction “R” and diffusion “D” mechanism in Table 2) compared with the experimental master plot $P(u)/P(u)_{0.5}$ at 20 °C/min. With reference to Figures 3a, 3b and 3c, the most consistent model is the reaction-order type $(1-\alpha)^n$ with n=16 (Fn=F16 in Table 2) for conversions below 0.5, while for conversions

between 0.5 and 0.7 the reaction mechanism is the reaction-order type with n=11.5 (F11). At higher conversion values (between 0.7 and 0.95) it is not possible to determine a single function describing the experimental data: the type of reaction mechanism remains the same, but the reaction order decreases to 8. The F reaction order model suggests that the main mechanism depends on the concentration of the remaining reactants while other variables, such as the geometry and surface of the particle and matter transfer by diffusion, are negligible [58]. As shown in Figures 3d, 3e and 3f, *Te* microalga has the same behaviour with a reaction-order type mechanism with n=17 (F17) below the conversion 0.4 and F11 between the conversion of 0.4 and 0.65. For values higher than 0.65 the reaction mechanism varies according to the conversion and the reaction order decreased up to 9. As shown in Figures S5, S6 and S7, the same behaviour has been found for combustion, partial and full oxy-combustion processes, for both the microalgae. These results suggest that it is not possible to define any unique function that describes the entire kinetic processes, but a conversion region where a single function describes the experimental data can be identified (Table 4). This is because the master plot method uses the average value of activation energy in order to predict the reaction mechanism. Nevertheless, there are conversion ranges where the reaction mechanism is unique and the corresponding value of the pre-exponential factor *A* can be determined plotting $[(1-\alpha)^{(1-n)}-1]/(n-1)$ versus $P(u)E/(\beta R)$ by least-square fitting procedure; the pertinent results are shown in Figure 4 for pyrolysis and Figure S8 for combustion, partial and full oxy-combustion conditions. Table 4 reports the kinetic parameters results of microalgae for all the studied processes. These ranges are related to the degradation of the main

pseudo-components that compose microalgae: proteins, carbohydrates and lipids. As shown, the type of reaction mechanism for all processes is the same and depends on reagent concentration in the surface (*F*). The reaction order *n* and pre-exponential factor *A* increase with oxygen concentration (FOX > POX > ABC > PYR) for *Te*, but they change remarkably for *Na* (POX > PYR > FOX > ABC). The trend is the same achieved for the activation energy, as reported in the previous section.

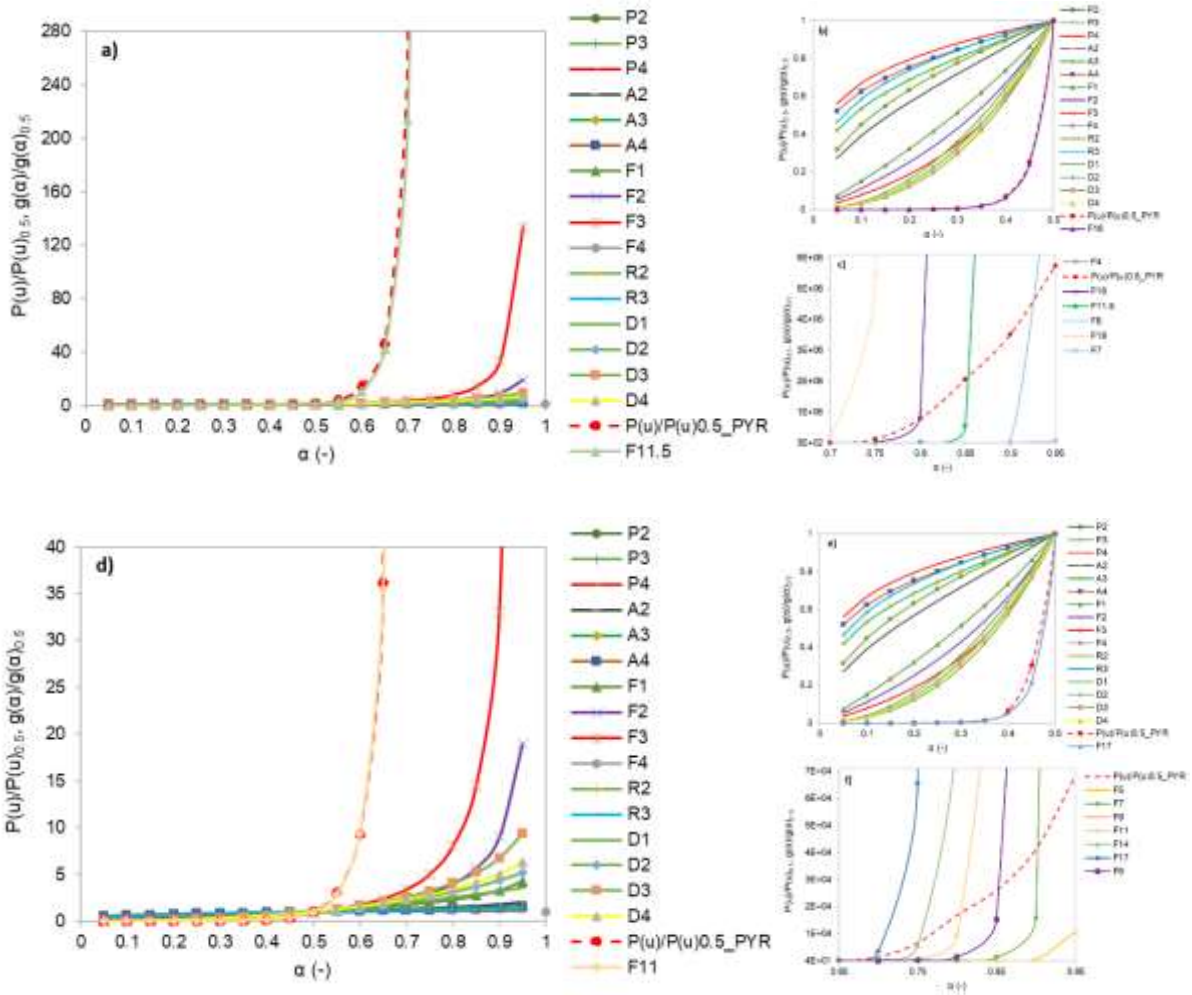

Figure 3. Experimental master plots $P(u)/P(u)_{0.5}$ and theoretical master plots $g(\alpha)/g(\alpha)_{0.5}$ comparison between $0.05 \leq \alpha \leq 0.95$, $0.05 \leq \alpha \leq 0.5$ and $0.7 \leq \alpha \leq 0.95$ of Na (a, b, and

c), and between 0.05 ≤ α ≤ 0.95, 0.05 ≤ α ≤ 0.5 and 0.65 ≤ α ≤ 0.95 of Te (d, e and f), in pyrolysis process at β=20 °C/min.

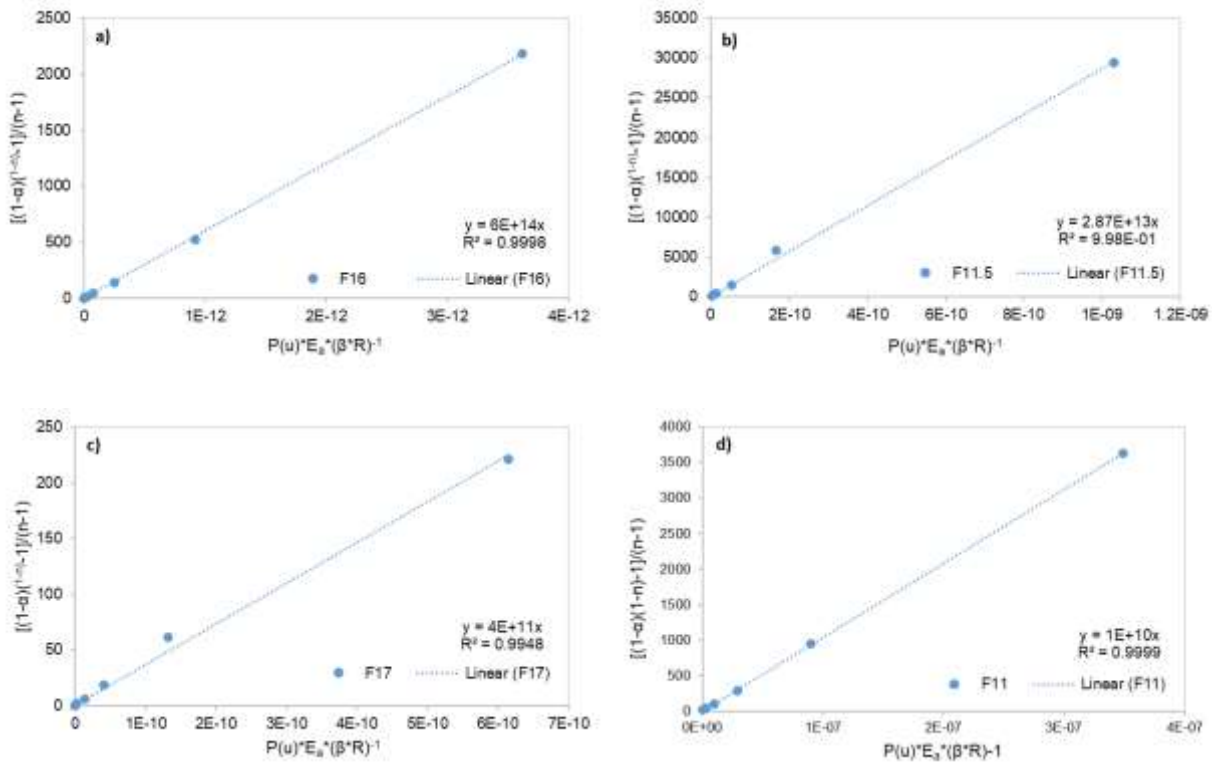

Figure 4. Plots of $g(\alpha)= [(1-\alpha)^{(1-n)}-1]/(n-1)$ versus $P(u)E_a/(\beta R)$ between 0.05 ≤ α ≤ 0.5 and 0.5 ≤ α ≤ 0.7 for Na (a and b), and between 0.05 ≤ α ≤ 0.4 and 0.4 ≤ α ≤ 0.65 for Te (c and d) in pyrolysis process at β=20°C/min.

Table 4. Kinetic parameters and reaction mechanism obtained for Na and Te in pyrolysis, combustion, partial oxy-combustion and full oxy-combustion processes using the single-step reaction approach.

Process	*Sample*	*α (-)*	*E_a (kJ/mol)*	*β (°C/min)*	*Reaction mechanism*	*n*	*A (1/s)*	*R^2*
PYR	Na	0.05-0.5	163.20	20	F	16	6.01E+14	0.9998
		0.5-0.7	163.20	20	F	11.5	2.87E+13	0.9993
	Te	0.05-0.4	124.00	20	F	17	3.66E+11	0.9948

		0.4-0.65	124.00	20	F	11	1.04E+10	0.9999
ABC	Na	0.05-0.6	104.54	20	F	12.5	5.18E+08	0.9995
	Te	0.05-0.6	132.19	20	F	14.5	5.49E+11	0.9996
POX	Na	0.05-0.6	132.40	20	F	18	3.41E+12	0.9998
	Te	0.05-0.6	222.29	20	F	28	1.82E+23	0.9999
FOX	Na	0.05-0.6	113.14	20	F	13	5.34E+09	0.9985
	Te	0.05-0.6	256.38	20	F	32.5	1.41E+27	0.9999

3.2.2 Kinetic parameters determined for a multi-step mechanism

As shown in the previous section, the use of a single-step mechanism reaction to study thermal decomposition behaviour of microalgae often does not allow to characterise the process with a single reaction mechanism in the whole conversion range. This can be observed in Figure 1, where the asymmetric DTG profiles show that more than one devolatilization and decomposition stage occur. As a result, several parallel decomposition reactions should be taken into account and the kinetic must be assessed from the sum of the decomposition kinetics of all the reactions. The global DTG curves for every heating rate and each operative conditions (pyrolysis, combustion, partial oxy-combustion and oxy-combustion) have been deconvoluted into pseudo-components (moisture, light hydrocarbons, carbohydrates, proteins, lipids and biochar); the pertinent results, all obtained at a heating rate of 20 °C/min (chosen as reference) are reported in Figure 5 for both the microalgae samples (*Na* on the left side and *Te* on the right side).

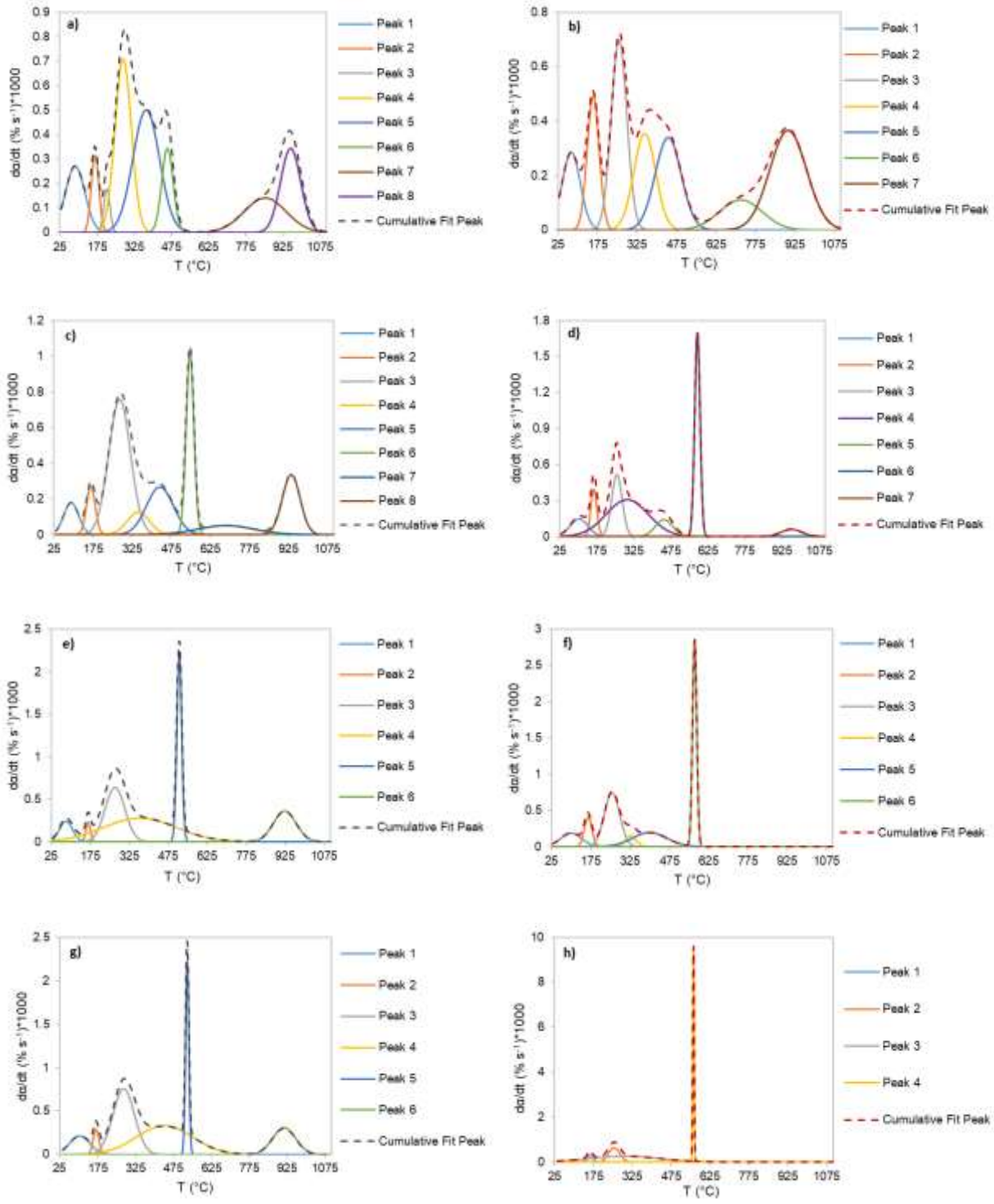

Figure 5. Comparison between the cumulative and estimated curves of each pseudo-component of Na (left side) and Te (right side), respectively, at 20 °C/min in

pyrolysis (a and b), combustion (c and d), partial oxy-combustion (e and f) and full oxy-combustion (g and h) processes.

The obtained data provide a satisfactory outcome, with R^2 correlation factor ranging from 0.9722 to 0.9951. Thanks to the deconvolution study, the identification of microalgae components has been performed. In all the deconvolution curves of Figure 5, peaks at temperature below 200 °C are attributed to moisture (cellular and externally bound water), and to the release of volatile matter; only during the oxy-combustion process (95 vol.% of oxygen), the first peak is not revealed for both the microalgae. After 200 °C, in the region between 200 and approximately 500 °C, the main components of the samples including carbohydrates, proteins and lipids underwent different decomposition mechanisms including depolymerization, decarboxylation and cracking [73,74]. Microalgae carbohydrates are complex and include a mixture of neutral sugars, amino sugars, and uronic acid [75]. In particular, the first zone corresponds to the decomposition of carbohydrates followed by the decomposition of proteins and soluble polysaccharides, and, finally, the decomposition of insoluble polysaccharides and crude lipids [76]. In the final stage, above 600 °C, the production of char takes place and – depending on the process – at higher temperature, the degradation of carbonaceous matters occurs. Relative mass loss contributions of each pseudo-components, *i.e.* the relative fraction of the area under the deconvoluted peak, have been calculated and the pertinent results gathered in Table 5.

Table 5. Average relative mass loss contribution of the pseudo-components for the Na and Te.

Process		*Moisture (%)*		*Light HC** (%)		*Carbohydrate (%)*		*Proteins (%)*		*Lipids (%)*		*Biochar (%)*	
		Na	Te	Na	Te	Na	Te	Na	Te	Na	Te	Na	Te
PYR	0% O_2	9.3	9.4	5.7	9.3	24.2	17.1	27.8	23.3	7.0	8.3	26.1	32.6
ABC	21% O_2	5.3	7.7	4.8	7.0	34.5	16.3	5.8	33.6	13.9	7.3	35.7	29.1
POX	58% O_2	5.5	9.2	1.8	7.1	21.7	18.7	-	24.3	38.0	17.6	33.1	23.1
FOX	95% O_2	-	-	4.5	4.6	15.9	17.2	3.5	-	53.8	46.9	22.3	31.4

*Light HC: Light hydrocarbons

It is worth noting that the obtained mass loss contribution stems from the average of all the heating rates (5, 10, 15, 20 and 40 °C/min). A careful analysis of these results shows that no simple correlation exists between the mass loss contributions of the pseudo-components and the reactive atmosphere, even if a specific trend can be established. It is possible to observe a clear difference between pyrolysis and all the combustion regimes (21, 58 and 95 vol.% of oxygen) for both the samples. Concerning the Na microalga, the relative mass loss contribution of carbohydrates decreases (from 34.5% to 15.9%) with the increase of the oxygen concentration (from 21 to 95 vol.%). On the contrary, the relative mass loss contribution of lipids is almost four-times higher when oxygen concentration increases from 21% to 95% by volume; the relative mass loss contribution of proteins appears to be constant with the increase of oxygen. On the other hand, Te microalga seems to follow a different behaviour; the relative mass loss contribution of carbohydrates remains constant with the increase in oxygen concentration; the relative mass loss contribution of lipids increases (from 7.3% to 46.9%) with increasing oxygen concentration (from 21% to 95% by volume). The

difference in thermal decomposition behaviour here presented could be ascribed to the differences in the natural structural and chemical characteristics leading to different mechanisms of decomposition.

Based on these deconvoluted curves, the kinetic parameters are evaluated. The activation energy of each pseudo-component has been calculated using Kissinger's method from the maximum temperature of the peak; the obtained results are reported in Table 6.

Table 6. Average value of activation energy for each pseudo-component evaluated by Kissinger's method for the Na and Te.

Process		*Moisture (kJ/mol)*		*Light HC** *(kJ/mol)*		*Carbohydrate (kJ/mol)*		*Proteins (kJ/mol)*		*Lipids (kJ/mol)*		*Biochar (kJ/mol)*	
		Na	Te	Na	Te	Na	Te	Na	Te	Na	Te	Na	Te
PYR	0% O_2	310	42	390	102	263	207	194	46	211	81	-	512
ABC	21% O_2	22	32	150	148	143	33	108	79	34	12	233	191
POX	58% O_2	55	96	130	224	588	271	-	74	139	23	696	94

*Light HC: Light hydrocarbons

Each pseudo-component shows different E_a values, confirming that every process involves a multi-step mechanism and consequently, the decomposition of each component is represented by its respective kinetic parameter. In general, it is noted a higher value of activation energy of each pseudo-component in pyrolysis compared to air-blown combustion and lower activation energy values of *Te* compared to *Na*. A reaction with lower apparent activation energy requires less energy to break down the chemical bonds between atoms resulting in a faster reaction rate. It was not possible

the assessment of E_a for the oxy-combustion process (95 v/v.% of oxygen) due to the presence of a poor resolution overlapped peak or high-intensity peaks (in the case of biochar). Furthermore, at the end of the reaction, the residual solid shows high thermal stability and results in an increase in the energy required to break the bonds.

All in all, two factors directly affect the reactivity of microalgae samples, which is correlated with the obtained kinetic parameters. Firstly, the biochemical composition of the samples has a main role in the process [64]. A high content of a certain major component (carbohydrates, lipids or proteins) will provide a higher reactivity in the corresponding temperature range. Secondly, ash plays a catalytic role in the process [77]. The possible presence of inorganic matter in *Te* sample seems to catalyse the process and, as a result, the obtained E_a values are in principle lower than those of the *Na* microalga. Comparing the reactivity in terms of activation energy, and irrespective of the reactive atmosphere, it can be observed that *Te* sample is more reactive than *Na* sample. This behaviour could be ascribed to the catalytic effect of ash, associated to the presence of individual elements rather than to their quantities. In this sense, the activity of Ca seemed to be more influential than other metals such as K or Mg as reported in literature [78].

Based on the findings of the present study, *Te* microalga, with a lower activation energy, appears to be more suitable than *Na* even though for biofuel production a high volatiles amount and low ash content is required; from this point of view, *Na* appears to be more promising respect to *Te* microalga. These results provide useful information for designing a pyrolytic or combustion processing system using different microalgae as feedstock.

Using the activation energy values of main microalgae components (carbohydrates, proteins, lipids and biochar), the pre-exponential factor (*A*) and reaction mechanism ***f(α)*** for each kinetic process at the maximum value of the reaction rate (which corresponds to the maximum weight loss peaks) have been determined. Table 7 presents the kinetics parameters obtained with parallel reactions scheme (discussed in section A1.4 of the Supplementary material). The results suggest that the thermal behaviour is strongly influenced by the composition of the biomass materials and there are clear differences in the kinetics of pyrolysis, combustion and partial oxy-combustion between *Na* and *Te* microalgae. The kinetic profiles can be interpreted as the combined effects of reaction-order (*F*), nucleation (*A*), exponential nucleation (*P*) and geometrical contraction (*R*) mechanisms.

Table 7. Kinetic parameters and reaction mechanism obtained for Na and Te in pyrolysis, combustion and partial oxy-combustion processes at the maximum weight loss peak (*p*), using the multi-step reaction approach (CB=Carbohydrates, PT= Proteins, LP= Lipids, BC= Biochar).

Process	*Sample*	*Peak*	$(d\alpha/dt)_p$ *(% s^{-1})*1000)*	T_p *(°C)*	E_a *(kJ/mol)*	A_p *(1/s)*	n_p	*Reaction mechanism*
PYR	Na	3 (CB)	0.18	213.4	114.48	5,07E+10	1,3	F
		4 (CB)	0.71	279.1	148.99	2,73E+12	1,8	F
		5 (PT)	0.50	373.4	194.22	2,33E+14	4	F
		6 (LP)	0.34	457.0	211.59	1,51E+13	1	F
		7 (BC)	0.18	853.5	-	-	-	-
		8 (BC)	0.39	956.1	-	-	-	-
ABC	*Na*	3 (CB)	0.75	276.2	143.25	1.97E+12	4	F
		4 (PT)	0.12	347.6	107.66	1.79E+07	2	F
		5 (LP)	0.26	430.9	34.17	6.38E+00	2.5	A
		6 (BC)	1.01	547.2	25.69	9.76E-01	12	P
		7 (BC)	0.05	683.4	24.19	5.49E-01	2.5	A
		8 (BC)	0.33	934.6	182.82	5.39E+05	2	A
POX	*Na*	3 (CB)	0.64	268.9	588.38	1.38E+59	13	F
		4 (PT)	0.28	364.6	139.34	5.81E+10	10	F
		5 (LP)	2.20	517.1	212.33	2.40E+11	3	R

		6 (BC)	0.36	921.9	483.62	3.01E+19	3	F
PYR	*Te*	3 (CB)	0.69	256.5	206.93	5.47E+18	0.6	F
		4 (PT)	0.35	353.2	45.81	4.51E+01	2	A
		5 (LP)	0.34	442.7	81.52	8.78E+03	1	F
		6 (BC)	0.11	719.7	512.47	4.93E+26	8	F
		7 (BC)	0.36	898.9	240.02	4.24E+08	2	F
ABC	*Te*	3 (CB)	0.52	257.3	32.59	8.59E+00	3	R
		4 (PT)	0.31	300.1	78.73	1.12E+06	5	F
		5 (LP)	0.14	448.8	12.55	2.79E-01	4	P
		6 (BC)	1.69	587.9	191.22	7.71E+08	3	R
		7 (BC)	-	-	-	-	-	-
POX	*Te*	3 (CB)	0.74	255.1	271.45	2.55E+26	6	F
		4 (PT)	0.15	326.8	74.07	4.02E+04	2	A
		5 (LP)	0.19	399.7	23.28	1.73 E+00	3	A
		6 (BC)	2.85	571.7	94.28	7.49E+03	9	P

4. Conclusions

The kinetic performance comparison of *Na* and *Te* microalgae during pyrolysis and combustion with air, enriched air and oxygen has allowed to determine the kinetic triplet (activation energy, E_a, the reaction order, n, and the pre-exponential factor, A) and to assess the reaction mechanism.

Several parallel decomposition reactions have been taken into account, and the kinetic has been assessed from each decomposition kinetic of the pseudo-components.

Na and *Te* microalgae present an activation energy (expressed as the average value calculated with FWO, KAS and Starink models) of 163.2 and 124.0 kJ/mol for pyrolysis, 104.54 and 132.12 kJ/mol for combustion, 130.87 and 207.66 kJ/mol for partial oxy-combustion, 113.14 and 256.38 kJ/mol for full oxy-combustion, respectively. It can be noticed that the activation energy of *Te* increases with increased oxygen concentration, whereas the activation energy of *Na* changes remarkably from pyrolysis to combustion and from partial to full oxy-combustion processes.

The kinetic profiles can be interpreted as the combined effects of reaction-order (*F*), nucleation (*A*), exponential nucleation (*P*) and geometrical contraction (*R*) mechanisms. Based on the findings of the present study, *Te* microalga, with a lower activation energy, appears to be more suitable than *Na* even though for biofuel production a high volatiles amount and low ash content is required; from this point of view, *Na* appears to be more promising respect to *Te* microalga. Moreover, the kinetic results here reported represent useful information for designing a microalgae-fed pyrolytic or combustion processing system.

Conflicts of interest

The authors declare that there is no conflict of interest.

Acknowledgements

The Sotacarbo contribution in this work has been carried out within the “Centre of Excellence on Clean Energy” research project (D83C17000370002) led by Sotacarbo and funded by the Regional Government of Sardinia (FSC 2014-2020).

References

[1] International Energy Agency. World Energy Outlook 2019. Paris, France, 2019.

[2] Ward C, Goldstein H, Maurer R, Thimsen D, Sheets BJ, Hobbs R, Isgrigg F, Steiger R, Revay Madden D, Porcu A, Pettinau A. Making coal relevant for small scale applications: Modular gasification for syngas/engine CHP applications in challenging environments. Fuel 2020;267:117303.

[3] Lamaison N, Collette S, Vallée M, Bavière R. Storage influence in a combined biomass and power-to-heat district heating production plant. Energy 2019;186:115714.

[4] Johansson C, Lehtveer M, Göransson L. Biomass in the electricity system: A complement to variable renewables or a source of negative emissions? Energy 2019;168:532-541.

[5] Goffé J, Ferrasse JH. Stoichiometry impact on the optimum efficiency of biomass conversion to biofuels. Energy 2019;170:438-458.

[6] Sun X, Atiyeh HK, Li M, Chen L. Biochar facilitated bioprocessing and biorefinery for productions of biofuel and chemicals: A review. Bioresource Technol. 2020;295:122252.

[7] Bach QV, Chen WH, Lin SC, Sheen HK, Chang JS. Wet torrefaction of microalga Chlorella vulgaris ESP-31 with microwave-assisted heating. Energy Convers. Manag. 2017;141:163-170.

[8] Maity JP, Bundschuh J, Chen CY, Bhattacharya P. Microalgae for third generation biofuel production, mitigation of greenhouse gas emissions and wastewater treatment: Present and future perspectives – A mini review. Energy 2014;78:104-113.

[9] Llamas M, Magdalena JA, Tomás-Pejó E, González-Fernández C. Microalgae-based anaerobic fermentation as a promising technology for producing biogas and microbial oils. Energy 2020;206:118184.

[10] He Y, Zhang B, Guo S, Guo Z, Chen B, Wang M. Sustainable biodiesel production from the green microalgae Nannochloropsis: Novel integrated processes from

cultivation to enzyme-assisted extraction and ethanolysis of lipids. Energy Convers. Manag. 2020;209:112618.

[11] Sati H, Mitra M, Mishra S, Baredar P. Microalgal lipids extraction strategies for biodiesel production: A review. Algal Res. 2019;38:101413.

[12] Chua ET, Schenk PM. A biorefinery for Nannochloropsis: Induction, harvesting, and extraction of EPA-rich oil and high-value proteins. Bioresource Technol. 2017;244:1416-1424.

[13] Lee XJ, Ong HC, Gan YY, Chen WH, Indra Mahlia TM. State of art review on conventional and advanced pyrolysis of macroalgae and microalgae for biochar, bio-oil and bio-syngas production, Energy Convers. Manag. 2020;210:112707.

[14] Kawale HD, Kishore N. Comparative study on pyrolysis of Delonix Regia, Pinewood sawdust and their co-feed for plausible bio-fuels production. Energy 2020;203:117921.

[15] Durak H. Thermochemical conversion of Phellinus pomaceus via supercritical fluid extraction and pyrolysis processes. Energy Conv. Manag. 2015;99:282-298.

[16] Durak H, Genel S. Catalytic hydrothermal liquefaction of lactuca scariola with a heterogeneous catalyst: The investigation of temperature, reaction time and synergistic effect of catalysts. Bioresource Technol. 2020;309:123375.

[17] Durak H, Aysu T. Thermochemical liquefaction of algae for bio-oil production in supercritical acetone/ethanol/isopropanol. J Supercritical Fluids 2016;111:179-198

[18] Ceylan S, Kazan D. Pyrolysis kinetics and thermal characteristics of microalgae Nannochloropsis oculata and Tetraselmis sp. Bioresource Technol. 2015;187:1-5.

[19] Gautam R, Vinu R. Non-catalytic fast pyrolysis and catalytic fast pyrolysis of Nannochloropsis oculata using Co-Mo/γ-Al_2O_3 catalyst for valuable chemicals. Algal Res. 2018;34:12-24.

[20] Li F, Srivatsa SC, Bhattacharya S. A review on catalytic pyrolysis of microalgae to high-quality bio-oil with low oxygeneous and nitrogenous compounds. Renew. Sust. Energ. Rev. 2019;108:481-497.

[21] Fermoso J, Corbet T, Ferrara F, Pettinau A, Maggio E, Sanna A. Synergistic effects during the co-pyrolysis and co-gasification of high volatile bituminous coal with microalgae. Energy Convers. Manag. 2018;164:399-409.

[22] Wu Z, Li Y, Zhang B, Yang W, Yang B. Co-pyrolysis behavior of microalgae biomass and low-rank coal: Kinetic analysis of the main volatile products. Bioresource Technol. 2019;271:202-209.

[23] Chang G, Miao P, Wang H, Wang L, Hu X, Guo Q. A synergistic effect during the co-pyrolysis of Nannochloropsis sp. and palm kernel shell for aromatic hydrocarbon production. Energy Convers. Manag. 2018;173:545-554.

[24] Tang Z, Chen W, Chen Y, Yang H, Chen H. Co-pyrolysis of microalgae and plastic: Characteristics and interaction effects. Bioresource Technol. 2019;274:145-152.

[25] Choi HI, Lee JS, Choi JW, Shin YS, Sung YJ, Hong ME, Kwak HS, Kim CY, Sim SJ. Performance and potential appraisal of various microalgae as direct combustion fuel. Bioresource Technol. 2019;273:341-349.

[26] Plis A, Lasek J, Skawińska A. Kinetic analysis of the combustion process of Nannochloropsis gaditana microalgae based on thermogravimetric studies. J. Anal. Appl. Pyrol. 2017;127:109-119.

[27] Ye B, Zhang R, Cao J, Lei K, Liu D. The study of co-combustion characteristics of coal and microalgae by single particle combustion and TGA methods. J. Energy Inst. 2020;93:508-517.

[28] Dai J, Sokhansnji S, Grace JR, Bi X, Kim CJ, Melin S. Overview and some issues related to co-firing biomass and coal. Can. J. Chem. Eng. 2008;86:367-386.

[29] Liu Z, Balasubramanian R. A comparison of thermal behaviors of raw biomass, pyrolytic biochar and their blends with lignite Bioresource Technology 2013;146:371-378.

[30] Khan AA, Jong W, Jansens PJ, Spliethoff H. Biomass combustion in fluidized bed boilers: potential problems and remedies. Fuel Process. Technol. 2009;90:21-50.

[31] Saidur R, Abdelaziz EA, Demirbas A, Hossain MS, Mekhilef S. A review on biomass as a fuel for boilers. Renew. Sust. Energy Rev. 2011;15:2262-2289.

[32] Radmanesh R, Courbariaux Y, Chaouki J, Guy C. A unified lumped approach in kinetic modeling of biomass pyrolysis. Fuel 2006;85:1211-1220.

[33] Senneca O. Kinetics of pyrolysis, combustion and gasification of three biomass fuels. Fuel Process. Technol. 2007;88:87-97.

[34] Bach QV, Chen WH. A comprehensive study on pyrolysis kinetics of microalgal biomass. Energy Convers. Manag. 2017;131:109-116.

[35] Di Blasi C. Modelling chemical and physical processes of wood and biomass pyrolysis. Prog. Energ. Combust. 2008;34:47-90.

[36] López-González D, Fernandez-Lopez M, Valverde JL, Sanchez-Silva L. Pyrolysis of three different types of microalgae: Kinetic and evolved gas analysis. Energy 2014;73:33-43.

[37] Bui HH, Tran KQ, Chen WH. Pyrolysis of microalgae residues – a kinetic study. Bioresource Technol. 2016;199:362-366.

[38] Soria-Verdugo A, Tomasi Morgano M, Mätzing H, Goos E, Leibold H, Merz D, Riedel U, Stapf D. Comparison of wood pyrolysis kinetic data derived from thermogravimetric experiments by model-fitting and model-free methods. Energy Convers. Manag. 2020;212:112818.

[39] Ali I, Bahadar A. Red Sea seaweed (Sargassum spp.) pyrolysis and its devolatilization kinetics. Algal Res. 2017;21:89-97.

[40] Vega F, Camino S, Camino JA, Garrido J, Navarrete B. Partial oxy-combustion technology for energy efficient CO_2 capture process. Appl. Energy 2019;253:113519.

[41] Cau G, Tola V, Ferrara F, Porcu A, Pettinau A. CO_2-free coal-fired power generation by partial oxy-fuel and post-combustion CO_2 capture: Techno-economic analysis. Fuel 2018;214:423-435.

[42] Zainan NH, Srivatsa SC, Bhattacharya S. Catalytic pyrolysis of microalgae Tetraselmis suecica and characterisation study using in situ Synchrotron-based Infrared Microscopy. Fuel 2015;161:345-354.

[43] Blanco PH, Wu C, Onwudili JA, Williams PT. Characterisation and evaluation of Ni/SiO_2 catalysts for hydrogen production and tar reduction from catalytic steam

pyrolysis-reforming of refuse derived fuel. Appl. Catal. B: Environ. 2013;134-135:238-250.

[44] Fermoso J, Coronado JM, Serrano DP, Pizarro P. Pyrolysis of microalgae for fuel production. In: Gonzalez-Fernandez C, Muñoz R (eds) Microalgae- based biofuels bioprod. Woodhead Publishing, Elsevier Ltd, Duxford, 2017:259-282.

[45] Wang K, Brown RC. Catalytic pyrolysis of microalgae for production of aromatics and ammonia. Green Chem. 2013;15:675-681.

[46] Yuan T, Tahmasebi A, Yu J. Comparative study on pyrolysis of lignocellulosic and algal biomass using a thermogravimetric and a fixed-bed reactor. Bioresource Technol. 2015;175:333-341.

[47] Hames B, Scarlata C, Sluiter A., 2008. Determination of proteins content in biomass: laboratory analytical procedure (LAP). U.S. Department of Energy, National Renewable Energy Laboratory, report No. 42625, Golden, Clorado (USA), 2008. Available at http://www.nrel.gov/docs/gen/fy08/42625.pdf.

[48] Vyazovkin S, Chrissafis K, Di Lorenzo ML, Koga N, Pijolat M, Roduit B, Sbirrazzuoli N, Suñol JJ. ICTAC Kinetics Committee recommendations for collecting experimental thermal analysis data for kinetic computations. Thermochim. Acta 2014;590:1-23

[49] Mureddu M, Dessì F, Orsini A, Ferrara F, Pettinau A. Air- and oxygen-blown characterisation of coal and biomass by thermogravimetric analysis. Fuel 2018;212:626-637.

[50] Zou H, Zhang J, Liu J, Buyukada M, Evrendilek F, Liang G. Pyrolytic behaviors, kinetics, decomposition mechanisms, product distributions and joint optimization of Lentinus edodes stipe. Energy Convers. Manag. 2020;213:112858.

[51] Flynn JH, Wall LA. A Quick, direct method for the determination of activation energy from thermogravimetric data. Polym. Lett. 1966;4:323-328.

[52] Ozawa T. A new method of analyzing thermogravimetric data. B. Chem. Soc. Jpn. 1965;38:1881-1886.

[53] Kissinger HE. Variation of peak temperature with heating rate in differential thermal analysis. J. Res. Natl. Inst. Stan. 1956;57:217-221.

[54] Akahira T, Sunose T. Method of determining activation deterioration constant of electrical insulating materials. Research Report, Chiba Institute of Technology 1971;16:22-31.

[55] Starink MJ. A new method for the derivation of activation energies from experiments performed at constant heating rate. Thermochim. Acta 1996;288:97-104.

[56] Kissinger HE. Reaction kinetics in differential thermal analysis. Anal. Chem. 1957;29:1702-1706.

[57] Gotor FJ, Criado JM, Malak J, Koga N. Kinetic analysis of solid-state reactions: The universality of master plots for analyzing isothermal and nonisothermal experiments. J. Phys. Chem. A 2000;104:10777-10782.

[58] Khawam A, Flanagan DR. Solid-State Kinetic Models: Basics and Mathematical Fundamentals. J. Phys. Chem. B 2006;110:17315-17328.

[59] Vyazovkin S. Isoconversional Kinetics of Thermally Stimulated Processes. Springer International Publishing. In: Isoconversional Methodology (Chapter 2). 2015;27-62.

[60] Chen C, Ma X, Liu K. Thermogravimetric analysis of microalgae combustion under different oxygen supply concentrations. Appl. Energy 2011;88:3189-3196.

[61] Sanchez-Silva L, López-González D, Garcia-Minguillan AM, Valverde JL. Pyrolysis, combustion and gasification characteristics of Nannochloropsis gaditana microalgae. Bioresource Technol. 2013;130:321-331.

[62] Luo SY, Xiao B, Hu ZQ, Liu SM, Guan YW. Experimental study on oxygen-enriched combustion of biomass micro fuel. Energy 2009;34:1880-1884.

[63] Marcilla A, Gómez-Siurana A, Gomis C, Chápuli E, Catalá MaC, Valdés FJ. Characterization of microalgal species through TGA/FTIR analysis: Application to nannochloropsis sp. Thermochim. Acta 2009; 484:41–47.

[64] López-González D, Fernandez-Lopez M, Valverde JL, Sanchez-Silva L. Kinetic analysis and thermal characterisation of the microalgae combustion process by thermal analysis coupled to mass spectrometry. Appl. Energy 2014;114:227-237.

[65] Gai C, Liu Z, Han G, Peng N, Fan A. Combustion behavior and kinetics of low-lipids microalgae via thermogravimetric analysis. Bioresource Technol. 2015;181:148-154.

[66] Kay RA. Microalgae as food and supplement. Crit. Rev. Food Sci. Nutr. 1991;30:555-573.

[67] Liden AG, Berruti F, Scott D. A kinetics model for the production of liquids from the flash pyrolysis of biomass. Chem. Eng. Commun. 1998;65:207-221.

[68] Czernik S, Bridgwater AV. Overview of application of biomass fast pyrolysis oil. Energy Fuels 2004;18:590-598.

[69] Aboulkas A, El Harfi K. Study of the kinetics and mechanisms of thermal decomposition of moroccan tarfaya oil shale and its kerogen. Oil shale 2008;25:426.

[70] Slopiecka K, Bartocci P, Fantozzi F. Thermogravimetric analysis and kinetic study of poplar wood pyrolysis. Appl. Energy 2012;97:491-497.

[71] Fang MX, Shen DK, Li YX, Yu CJ, Luo ZY, Cen KF. Kinetic study on pyrolysis and combustion of wood under different oxygen concentrations by using TG-FTIR analysis. J. Anal. Appl. Pyrol. 2006;77:22-27.

[72] Munir S, Daood SS, Nimmo W, Cunliffe AM, Gibbs BM. Thermal analysis and devolatilization kinetics of cotton stalk, sugar cane bagasse and shea meal under nitrogen and air atmospheres. Bioresource Technol. 2009;100:1413-1418.

[73] Peng W, Wu Q, Tu P. Pyrolytic characteristics of heterotrophic Chlorella protothecoides for renewable bio-fuel production. J. Appl. Phycol. 2001;13:5-12.

[74] Peng W, Wu Q, Tu P, Zhao N. Pyrolytic characteristics of microalgae as renewable energy source determined by thermogravimetric analysis. Bioresource Technol. 2001;80:1-7.

[75] Templeton DW, Quinn M, Van Wychen S, Hyman D, Laurens LML. Separation and quantification of microalgal carbohydrates. J. Chromatogr. A 2012;1270:225-234.

[76] Aysu T, Maroto-Valer MM, Sanna A. Ceria promoted deoxygenation and denitrogenation of Thalassiosira weissflogii and its model compounds by catalytic in-situ pyrolysis. Bioresource Technol. 2016;208:140-148.

[77] Ross AB, Jones JM, Kubacki ML, Bridgeman T. Classification of macroalgae as fuel and its thermochemical behaviour. Bioresource Technol. 2008;99:6494-6504.

[78] Yorulmaz SY, Atimtay AT. Investigation of combustion kinetics of treated and untreated waste wood samples with thermogravimetric analysis. Fuel Process. Technol. 2009;90:939-946.